Hindawi Publishing Corporation
International Journal of Aerospace Engineering
Volume 2016, Article ID 6346742, 11 pages
http://dx.doi.org/10.1155/2016/6346742

Research Article

A Multiconstrained Ascent Guidance Method for Solid Rocket-Powered Launch Vehicles

Si-Yuan Chen and Qun-Li Xia

School of Aerospace Engineering, Beijing Institute of Technology, Beijing 100081, China

Correspondence should be addressed to Si-Yuan Chen; 0035@bit.edu.cn

Received 28 March 2016; Accepted 28 June 2016

Academic Editor: Kenneth M. Sobel

This study proposes a multiconstrained ascent guidance method for a solid rocket-powered launch vehicle, which uses a hypersonic glide vehicle (HGV) as payload and shuts off by fuel exhaustion. First, pseudospectral method is used to analyze the two-stage launch vehicle ascent trajectory with different rocket ignition modes. Then, constraints, such as terminal height, velocity, flight path angle, and angle of attack, are converted into the constraints within height-time profile according to the second-stage rocket flight characteristics. The closed-loop guidance method is inferred by different spline curves given the different terminal constraints. Afterwards, a thrust bias energy management strategy is proposed to waste the excess energy of the solid rocket. Finally, the proposed method is verified through nominal and dispersion simulations. The simulation results show excellent applicability and robustness of this method, which can provide a valuable reference for the ascent guidance of solid rocket-powered launch vehicles.

1. Introduction

Hypersonic glide vehicles (HGV) are among the significant means of ultra-long range and fast attacks in the future. A solid rocket-powered launch vehicle is characterized by storage stability, short launch preparation time, and quick launch ability; it is also widely applied as an HGV carrier [1]. A boost-glide vehicle is equipped with an unconventional trajectory and strong maneuverability compared with the traditional ballistic missile. "Glide-insertion" launch trajectory has recently elicited widespread concern [2]. The solid rocket shuts off at the verge of the dense atmosphere, and the HGV directly proceeds with long-distance glide by aerodynamic force after separation. The launch vehicles fly along a low trajectory in the atmosphere and have posed a new challenge to the ascent guidance of launch vehicles.

Researchers have performed many studies on the method for the ascent guidance of launch vehicles, which mainly include reference trajectory design and tracking and atmospheric and exoatmospheric guidance. The reference trajectory design mainly adopts the direct method of trajectory optimization [3]. The famous launch vehicle trajectory optimization software programs POST [4] and OTIS [5] have found a solution that relies on direct shooting and point collocation methods, respectively. The pseudospectral method [6–8] has recently attracted widespread attention and relevant research achievements have formed special optimization software, such as the renowned GPOPS [9]. Despite good convergence and high computing efficiency, the direct method faces difficulties in online real-time application, particularly in offline trajectory design. In the trajectory tracking guidance, Lu [10] developed a nonlinear trajectory tracking guidance algorithm that tracks the precomputed trajectory and guarantees the satisfaction of the angle of attack and normal force path constraints. Seywald and Cliff [11] used a neighboring optimal control-based feedback law to guide a two-stage launch vehicle.

The indirect method of trajectory optimization is used by a majority of researchers to investigate the closed-loop ascent guidance [3]. Early research focused on the exoatmosphere, and the most representative methods are iterative guidance mode [12], which is used for the Saturn V rocket, and powered explicit guidance [13], which is intended for space shuttles. The principle is to infer a semianalytical solution under certain approximate assumptions and to avoid extensive numerical computation by determining a quasi-optimal value. Scholars have also developed the endoatmospheric ascent guidance method. Brown and Johnson [14]

used a linearized aerodynamics model to obtain optimal control. A conventional shooting method and a homotopy procedure were used. However, reliable convergence was not always attained. Dukeman [15–17] developed a closed-loop ascent guidance algorithm, which adopts a multiple-shooting method to solve a two-point boundary-value problem and to obtain the optimal ascent thrust direction. Lu [18, 19] used the finite difference method to deal with endoatmospheric optimal guidance and presented a connection mode for the two algorithms of endoatmosphere and exoatmosphere. Problems in practical engineering application (i.e., large computing amount and inability to ensure convergence all the time) occur despite a considerable number of studies on endoatmospheric optimal closed-loop guidance.

In addition to using the closed-loop guidance method derived from optimal control theory, the exoatmosphere guidance of ballistic missiles tends to use Lambert guidance [20–22], which manipulates thrust direction by elliptic orbit equation in accordance with rocket and target positions. A solid rocket is not equipped with a thrust termination system to simplify the structure. The fuel must be completely consumed. Thus, an energy management method other than Lambert guidance must be employed to waste some of the rocket's excess energy. Patha and McGehee [23] developed an alternate attitude control energy management method, which is an open-loop guidance method and is only suitable for vacuum environment. Zarchan [24] proposed a general energy management method, which is a closed-loop guidance method. The vacuum flight assumption has minimal effect on guidance precision. However, HGV launch is free from the constraint of elliptic orbit. Traditional ballistic missile guidance and energy management methods are no longer applicable.

In terms of HGV launch issues, a majority of scholars consider that the rocket engine can be shut off, and exoatmospheric optimal guidance can be used for launch vehicle to ship it to an appropriate altitude with a desired velocity and flight path angle [2, 25]. Current literature has failed to develop unified and effective solutions to a HGV launch with solid rocket shut off by fuel exhaustion. Xu and Chen [26] developed a spline energy management guidance method but failed to limit the terminal altitude. To address this technical challenge, we have considered various methods, such as designing several groups of nominal trajectories offline and selecting an appropriate trajectory online to conduct the whole-phase tracking guidance based on the estimated terminal velocity and tracking the nominal trajectory in the first stage of launch vehicle and then tracking online generated trajectory after applying open-loop energy management in the second stage to achieve terminal constraint. However, the aforementioned methods are all limited by poor guidance accuracy and robustness. The final proposed method is featured by small calculated amount and good robustness; and it has a certain capacity which constrains the terminal angle of attack while satisfying the HGV separation requirements.

This paper is organized as follows: Section 2 presents the dynamics model and constraints for the ascent guidance problem. Section 3 optimizes and analyzes the ascent trajectory, which can be used for the tracking guidance of the first-stage rocket. Sections 4 and 5 introduce a spline guidance method and a bias energy management, respectively, which are both used for the second-stage rocket and are implemented together to achieve the HGV separation requirements. Following this, the proposed closed-loop guidance method is tested in Section 6. Finally, the conclusions are presented in Section 7.

2. Ascent Guidance Problem Formulation

2.1. Dynamics Model. Consider that the launch vehicle flies in a vertical plane formed between the launch and target position. Due to short flight time, the impact of earth rotation is negligible. The point-mass dynamics of the launch vehicle over a spherical earth is described by the following equations of motion [27]:

$$\dot{V} = \frac{T\cos\alpha - D}{m} - g\sin\gamma, \tag{1}$$

$$\dot{\gamma} = \frac{T\sin\alpha + L}{mV} - g\frac{\cos\gamma}{V} + V\frac{\cos\gamma}{h + R_0}, \tag{2}$$

$$\dot{h} = V\sin\gamma, \tag{3}$$

$$\dot{R} = V\cos\gamma\frac{R_0}{h + R_0}, \tag{4}$$

where V is the velocity, h is the height, R is the range, γ is the flight path angle, T is the thrust force, α is the angle of attack, R_0 is the average radius of the Earth, m is the mass of the launch vehicle, and $g = g_0(R_0/(h + R_0))^2$ is the gravity acceleration, where $g_0 = 9.81\,\mathrm{m/s^2}$. The terms L and D are the aerodynamic lift force and drag force, that is, $L = qS_{\mathrm{ref}}C_L$ and $D = qS_{\mathrm{ref}}C_D$, where $q = 0.5\rho V^2$ is the dynamic pressure, ρ is the atmospheric density, S_{ref} is the reference area of the launch vehicle, and C_L and C_D are the lift and drag coefficients, respectively [28]. This study examines a two-stage solid rocket launch vehicle with relevant parameters that are reported in Table 1, and its payload adopts CAV-H [29].

2.2. Ascent Trajectory Constraints. The bending moment caused by aerodynamic force is a significant consideration in the ascent trajectory. This path constraint is typically in the form of the following inequality:

$$|q\alpha| \le b_{\max}, \tag{5}$$

where $b_{\max}$ is a nonnegative constant. Equation (5) ensures that the large angle of attack does not appear when the launch vehicle flies through high dynamic pressure areas.

Moreover, control variable α is restricted within a certain range of value, and its angular rate constraint is considered. Thus, the control constraint models are given by

$$\begin{aligned} \alpha_{\min} \le \alpha \le \alpha_{\max}, \\ \dot{\alpha}_{\min} \le \dot{\alpha} \le \dot{\alpha}_{\max}, \end{aligned} \tag{6}$$

Table 1: Launch vehicle properties.

	Stage 1	Stage 2
Total mass (kg)	16500	7093
Propellant mass (kg)	15173	5826
Mass flow rate (kg/s)	253	89.6
Burn time (s)	60	65
Specific impulse (s)	260	290
Thrust force (N)	645000	248500
Reference area (m^2)	3	3

where the subscripts "min" and "max" denote the minimum and maximum acceptable values, respectively.

The mission requirements indicate that a solid rocket should meet height h_f^*, velocity V_f^*, and flight path angle γ_f^* constraints at the time of fuel exhaustion:

$$h\left(t_f\right) = h_f^*,$$
$$V\left(t_f\right) = V_f^*, \quad (7)$$
$$\gamma\left(t_f\right) = \gamma_f^*.$$

Since the separation of the HGV at the verge of a dense atmosphere, some scholars argue that the rocket should also meet the terminal angle of attack constraint α_f^* [26]:

$$\alpha\left(t_f\right) = \alpha_f^*. \quad (8)$$

Finally, the ascent guidance problem can be described as follows: the two-stage launch vehicle is vertically launched from the ground and the thrust direction is a uniquely controlled variable. The path and the controlled variable constraints should be satisfied during the flight process; additionally, a specified HGV separation condition should be met when the rocket fuel is exhausted.

3. Ascent Trajectory Analysis

This section uses optimization theory to analyze the ascent trajectory characteristics. The optimization problem is solved by a pseudospectral method using GPOPS. The method and its applications are presented [9].

In this study, a "glide-insertion" ascent trajectory is considered. It is restricted by the constraints of a bending moment $b_{\max} = 4500$ ps-deg, an angle of attack variation rate $|\dot{\alpha}| \leq 10^\circ/\text{s}$, and a flight path angle variation rate $|\dot{\gamma}| \leq 2^\circ/\text{s}$. The terminal height and flight path angle constraints are set as $h_f = 60$ km and $\gamma_f = 0^\circ$, respectively. The cost function is maximum velocity at solid rocket shut-off point, $J = \max V(t_f)$. A comparison of different ignition modes is presented as follows.

Case 1. The solid rocket adopts "burn-burn" ignition mode.

Case 2. The solid rocket adopts "burn-coast-burn" ignition mode, and the angle of attack is limited to $\alpha = 0^\circ$ at the first-stage rocket separation point to conduct the coasting flight of the second-stage rocket. The ignition time of the second-stage rocket is obtained by optimization.

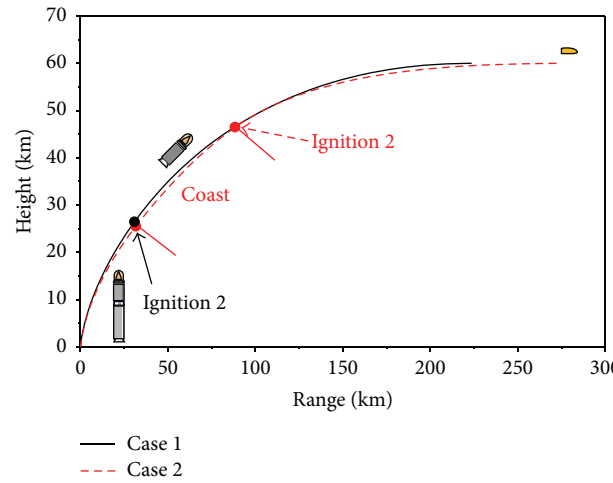

Figure 1: Ascent trajectories.

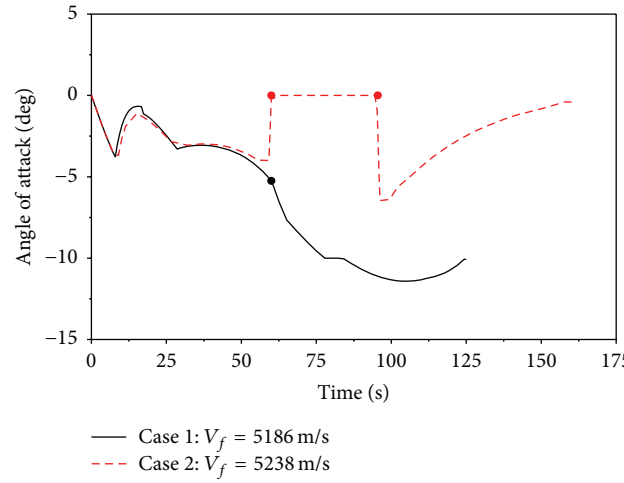

Figure 2: Angle of attack versus time.

Ascent trajectory and the corresponding angle of attack curves of the two cases are shown in Figures 1 and 2, respectively. The results show that Case 2 is superior to Case 1 regardless of range or terminal velocity. For the "glide-insertion" launch mission, the launch vehicle is required to turn agilely; the atmosphere at the altitude where the first-stage rocket shuts off is relatively dense. Therefore, the second-stage rocket ignited after a coasting flight to create a favorable flight environment for closed-loop guidance. As a result, the "burn-coast-burn" ignition mode of the solid rocket is employed for better performance of such launch mission.

This nominal trajectory can be used for tracking guidance of the first stage in order to guarantee a stable flight in the dense atmosphere. This paper does not provide a detailed introduction given that the tracking guidance method is relatively mature [27]. The second-stage rocket can use the

closed-loop guidance method proposed in the following sections to achieve terminal multiconstraint requirements.

4. Spline Guidance Method

The second-stage rocket ignited after reaching an appropriate altitude. The atmospheric density is relatively thin and has minimal influence on the rocket. Thus, aerodynamic force could be ignored in the derivation of the closed-loop guidance method. First, the second derivative of height with respect to time is taken as

$$\ddot{h} = \dot{V}\sin\gamma + V\cos\gamma\cdot\dot{\gamma}. \tag{9}$$

Equation (9) is simplified by (1) and (2) as follows:

$$\ddot{h} = \frac{T}{m}\sin(\alpha+\gamma) - g + V^2\frac{(\cos\gamma)^2}{h+R_0}. \tag{10}$$

Equations (3) and (10) show that the altitude rate $\dot{h}$ and altitude acceleration $\ddot{h}$ are related to height, velocity, flight path angle, and angle of attack. Thrust force is constant, dry mass of launch vehicle is known, and gravity is related to height. Therefore, the terminal constraint variables $(t_f, h_f, V_f, \gamma_f, \alpha_f)$ can be converted to $(t_f, h_f, \dot{h}_f, \ddot{h}_f)$.

The preceding analysis shows that spline curve, planned in the height-time (H-T) profile, can be used to solve the two-point boundary problem. The mission requirements indicate that different spline curves are used to solve the problem. If the constraints of terminal height, velocity, and flight path angle are considered, initial conditions (t_0, h_0) and $(t_0, \dot{h}_0)$, as well as terminal conditions (t_f, h_f) and $(t_f, \dot{h}_f)$, can be selected to obtain the reference trajectory by solving (11a), which is a cubic spline curve equation:

$$h_{\text{ref}}(t) = a_3(t-t_0)^3 + a_2(t-t_0)^2 + a_1(t-t_0) + a_0. \tag{11a}$$

If a terminal angle of attack constraint is found, that is, the constraint $\ddot{h}_f$ is included, the terminal condition $(t_f, \ddot{h}_f)$ can be further introduced to utilize (11b) quartic spline curve equation to solve the problem

$$h_{\text{ref}}(t) = a_4(t-t_0)^4 + a_3(t-t_0)^3 + a_2(t-t_0)^2 + a_1(t-t_0) + a_0. \tag{11b}$$

The initial conditions $(t_0, \ddot{h}_0)$ can be further added to obtain the reference trajectory and ensure the continuity of control command by solving (11c), which is a quintic spline curve equation

$$h_{\text{ref}}(t) = a_5(t-t_0)^5 + a_4(t-t_0)^4 + a_3(t-t_0)^3 + a_2(t-t_0)^2 + a_1(t-t_0) + a_0. \tag{11c}$$

Thus, the curve h_{ref} is determined by parameters $\mathbf{A} = [a_0, a_1, a_2, a_3, a_4, a_5]$, which are obtained by solving the system of linear equations. The nominal curves $\dot{h}_{\text{ref}}$ and $\ddot{h}_{\text{ref}}$ can be obtained by taking the first and second derivatives of h_{ref} with respect to time, respectively. The comparison of different spline curves is given as in Figure 3.

Figure 3 shows the change of different spline curves. The curve $\ddot{h}_{\text{ref}}$ plays a decisive role. $\dot{h}_{\text{ref}}$ and h_{ref} in time history could be determined once $\ddot{h}_{\text{ref}}$ is confirmed. Given the strong controllability of the rocket, the control constraint is not introduced in the curve planning and is conducted during the actual flight. The guidance command α_{ref} could be obtained by taking the inverse of (10):

$$\alpha_{\text{ref}} = \arcsin\left(\frac{1}{\dot{W}}\left(\ddot{h}_{\text{ref}} + g - V^2\frac{(\cos\gamma)^2}{h+R_0}\right)\right) - \gamma, \tag{12}$$

where $\dot{W} = T/m$ is axial acceleration, which can be measured by the inertial navigation system. Equation (12) shows that $\ddot{h}_{\text{ref}}$ has the most critical influence on α_{ref} given that the changes of γ and g are small in a short cycle.

Launch vehicle flight in accordance with α_{ref} can meet the planned curve $(h_{\text{ref}}, \dot{h}_{\text{ref}}, \ddot{h}_{\text{ref}})$ under relevant assumptions. However, when the aerodynamic effect and control constraints are introduced, the launch vehicle cannot fly along the planned curve, and the guidance command needs to be conducted with closed-loop correction. Closed-loop command generation involves two methods. One is prediction guidance, which constrains the current and terminal state through spline curve in each guidance period. Therefore, command α_{ref} is needed in real-time computing. This method is suitable for the problem without initial control constraint. This method cannot be used by (11c).

The other method is using trajectory tracking guidance, which takes aerodynamic influence and system uncertainty as disturbance factors to track online generated spline curves. The tracking control law can be described as

$$\begin{aligned} \alpha_c &= \alpha_{\text{ref}} + \delta\alpha, \\ \delta\alpha &= -\mathbf{K}\cdot\delta\mathbf{x}, \end{aligned} \tag{13}$$

where $\delta\mathbf{x} = (h \quad \dot{h})^{\text{T}} - (h_{\text{ref}} \quad \dot{h}_{\text{ref}})^{\text{T}}$. Feedback gains $\mathbf{K} = [k_1, k_2]$ can be calculated offline by linear quadratic regulator control law [25] and held constant. Constant gains cannot always ensure optimal performance. Nevertheless, they are suited for the situation in which the aerodynamic forces are negligible compared with the thrust force, and deviations from the nominal path are small.

Figure 4 shows the angle of attack curves with different spline guidance methods. The cubic and quartic spline prediction guidance do not introduce the initial angle of attack constraint. The beginning shows a convergence process that is caused by the deviation from guidance command and control constraint. Moreover, cubic spline prediction guidance does not introduce the terminal angle of attack constraint. The large command change occurs at the time close to the final time because the planned curve is updated in real time. The cubic spline tracking guidance first uses prediction guidance to eliminate initial deviation and then generates nominal trajectory to implement tracking guidance. Its terminal command is relatively smooth. The quintic spline tracking

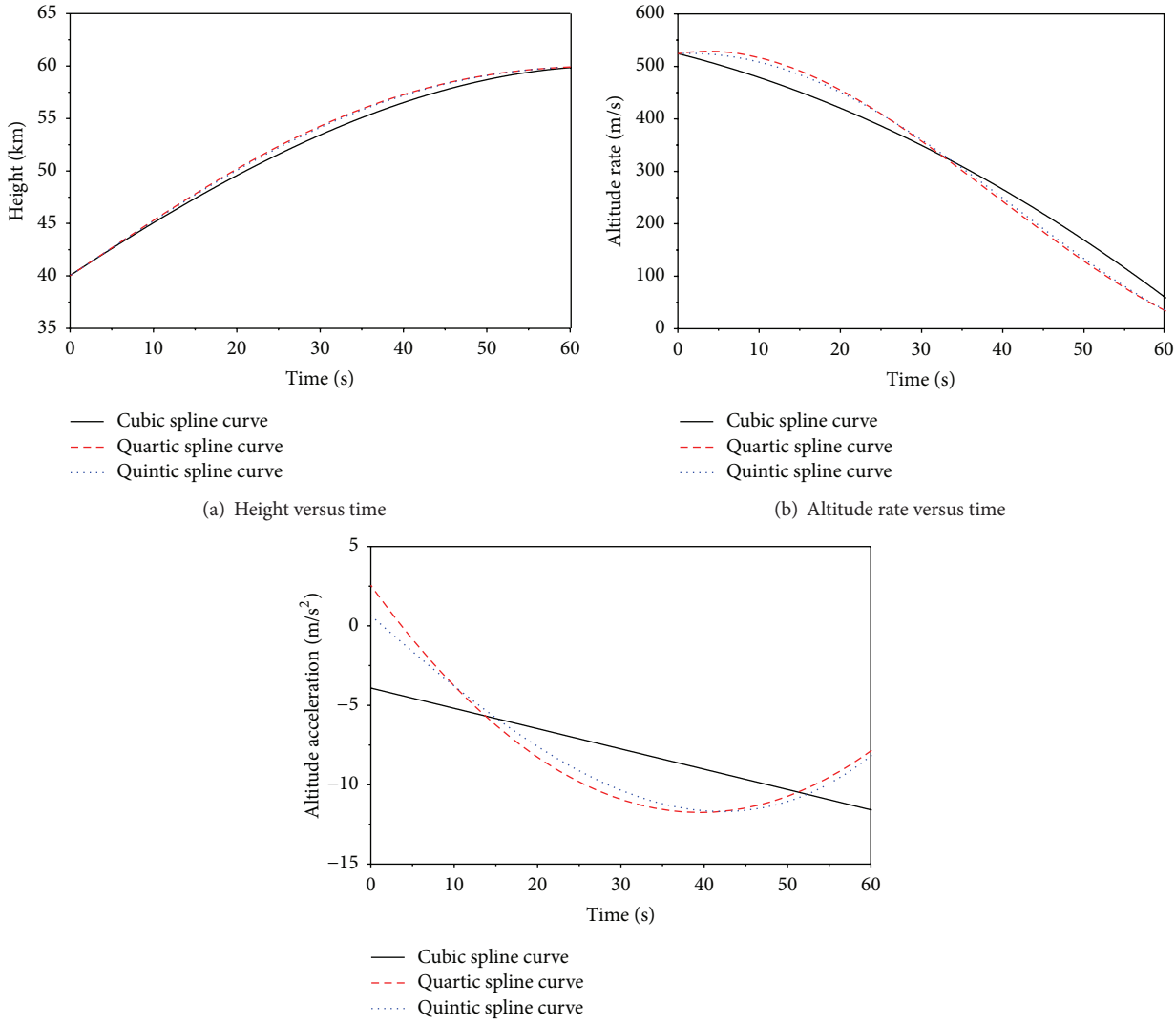

(a) Height versus time

(b) Altitude rate versus time

(c) Altitude acceleration versus time

FIGURE 3: Different spline curves.

guidance introduced the initial and terminal angle of attack constraints, and the guidance command changes slightly.

The closed-loop guidance based on spline curve is provided above. The design method adopts the equivalent state $(h_{\text{ref}}, \dot{h}_{\text{ref}}, \ddot{h}_{\text{ref}})$ rather than state (h, V, γ, α). If the terminal velocity $V(t_f)$ is not consistent with the expected speed V_f^*, the terminal constraints cannot be met even if the flight is conducted in accordance with the nominal curve. Therefore, a reasonable velocity control method should be conducted to achieve the desired state. An energy management strategy should be introduced for the solid rocket.

5. Bias Energy Management

The solid rocket is usually not equipped with a thrust termination system and shuts off by fuel exhaustion to reduce structure mass and improve reliability. The maximum velocity increment of the solid rocket can be expressed as [24]

$$W_f = \int_{\tau_0}^{\tau_f} \dot{W}\, dt = g_0 I_{\text{sp}} \ln \frac{m_0}{m_f}, \tag{14}$$

where τ_0 and τ_f represent the ignition and shut-off time of the rocket, respectively; m_0 and m_f are corresponding rocket mass; and I_{sp} is the engine specific impulse. The parameters on the right side of (14) can be confirmed in advance. The velocity produced by solid fuel is greater than the mission requirement. Therefore, energy management is needed to consume excess velocity.

The second-stage rocket guidance can be divided into the energy management and the closed-loop guidance phases. The energy management phase can be further divided into two phases. First, terminal velocity estimation method is

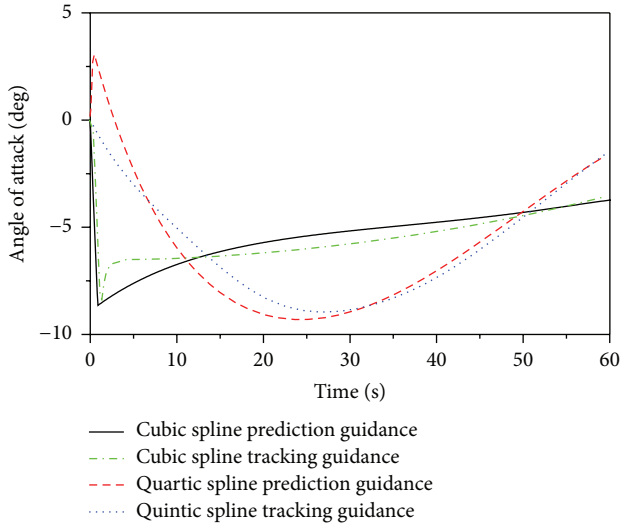

FIGURE 4: Different spline guidance methods.

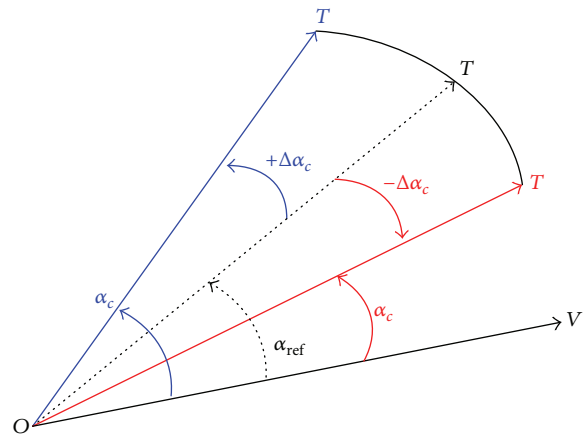

FIGURE 5: Schematic of thrust bias energy management.

used to calculate excess velocity. Second, energy management deceleration control is conducted based on excess velocity.

The analytical estimation method to estimate the terminal velocity is inaccurate under the effect of aerodynamic force. Therefore, the integral estimation method, which adopted closed-loop guidance, can be used. The closed-loop guidance command is also needed as a base command in the energy management process to ensure that the rocket is at a reasonable flight state. The analysis of the different spline guidance methods indicated that the cubic spline tracking guidance is suitable for estimating the terminal velocity without the need to update the curve in real time. Cubic spline prediction guidance can calculate the command in every guidance cycle, which is suitable as energy management base command.

The mass flow ratio $\dot{m}$ deviation is large. Although W_f is not affected, the deviation of τ_f occurs, which is a vital parameter for closed-loop guidance and terminal velocity estimation. Thus, τ_f and $\dot{m}$ estimation schemes should be introduced. Given that the axial velocity increment $W(t)$ is known at any time, the residual velocity increment can be expressed as

$$W_f - W(t) = g_0 I_{sp} \ln \frac{m_0 - \hat{\dot{m}}(t - \tau_0)}{m_f}. \tag{15}$$

Based on the inverse of (15), the estimated mass flow ratio $\hat{\dot{m}}$ is

$$\hat{\dot{m}} = \frac{m_0 - m_f \exp\left(\left(W_f - W(t)\right)/g_0 I_{sp}\right)}{t - \tau_0}. \tag{16}$$

The estimated shut-off time $\hat{\tau}_f$ can be expressed as

$$\hat{\tau}_f = \frac{m_0 - m_f}{\hat{\dot{m}}}. \tag{17}$$

The parameters $\hat{\dot{m}}$ and $\hat{\tau}_f$ can be computed in real time. Thus, excess velocity S is

$$S = V_{ref}\left(\hat{\tau}_f\right) - V_f^*, \tag{18}$$

where $V_{ref}(t)$ is velocity variation generated by spline guidance command. Equation (18) shows that $V_{ref}(t)$ must be changed to reduce S. Moreover, the only controllable variable of the solid rocket is thrust direction α_c.

Figure 5 shows that the actual thrust direction bias $\Delta\alpha_c$ is relative to the guidance command α_{ref} and forms horizontal projection $T\cos(\Delta\alpha_c)$ and vertical projection $T\sin(\Delta\alpha_c)$ in the guidance command direction. Vertical projection changes the current flight status to make the rocket deviate from the desired trajectory and thus affects the next cycle guidance command. Horizontal projection can be considered as the main factor that causes the change of $V_{ref}(t)$ at the current time given that the aerodynamic effect of the angle of attack is small. Therefore, the excess velocity variation rate $\dot{S}$ caused by $\Delta\alpha_c$ can be expressed as

$$\dot{S} = \frac{T}{m}\left(\cos\Delta\alpha_c - 1\right). \tag{19}$$

The excess velocity S is usually within a reasonable and controllable range. Therefore, S could be converged to zero at the expected time as long as the reasonable $\dot{S}$ change law is designed. When the dynamic processes and control constraints are not considered, an exponential decay curve, which takes time as the independent variable, is used to describe S:

$$S_c = S_0\left(\frac{\tau_e - t}{\tau_e - \tau_0}\right)^k \quad (k > 1), \tag{20}$$

where τ_e is the end time of energy management, S_0 is the excess velocity at time τ_0, k is exponential decay coefficient, and $k > 1$ means that, with the change of time, the excess velocity is reduced as nonlinear. The first-order derivative of time to S_c is

$$\dot{S}_c = -\frac{kS_0}{(\tau_e - \tau_0)}\left(\frac{\tau_e - t}{\tau_e - \tau_0}\right)^{k-1}. \tag{21}$$

The actual $\dot{S}$ cannot be in accordance with $\dot{S}_c$ because of the aerodynamic effect and control constraints. Therefore, $\dot{S}_c$ must be conducted with correction in real time. That is, $\tau_0 = t$ and $S_0 = S$. $\dot{S}_c$ is further simplified as

$$\dot{S}_c = -\frac{kS}{(\tau_e - t)}. \tag{22}$$

Equation (22) is substituted to the left side of (19) and inverse operation is conducted to obtain the bias command $\Delta\alpha_c$:

$$\left|\Delta\alpha_c\right| = \arccos\left(\frac{\dot{S}_c}{\dot{W}} + 1\right). \tag{23}$$

Equation (23) shows that the sign of $\Delta\alpha_c$ can be either positive or negative, which means that the thrust deflection direction can be located on both sides of α_{ref}. In the energy management process, the rocket deviates from the desired path given that bias $\Delta\alpha_c$, which always exists between α_c and α_{ref}. α_{ref}, is increased or decreased constantly if unilateral bias is adopted during the entire process. The large α_{ref} is not conducive to consume S given the constraint of α_c. Therefore, the bias command reversal strategy should be introduced. Repeated reversals should be avoided given that energy management time usually does not last long, and control constraint exists. Therefore, a simple and efficient single reversal strategy is proposed that almost equally distributes the energy management time on both sides. Finally, energy management command and reversal strategy are shown in

$$\alpha_c = \alpha_{\text{ref}} + k_{\text{sgn}} \cdot \left|\Delta\alpha_c\right|, \quad \left(\alpha_{\max} \le \alpha_c \le \alpha_{\min}\right), \tag{24}$$

$$k_{\text{sgn}} = \begin{cases} \text{sgn}\left(\alpha_{\text{ref}}\left(\tau_0\right)\right), & \tau_0 \le t < \tau_0 + 0.5\Delta\tau_E - \tau_{\text{Tra}}, \\ -\text{sgn}\left(\alpha_{\text{ref}}\left(\tau_0\right)\right), & \tau_0 + 0.5\Delta\tau_E - \tau_{\text{Tra}} \le t \le \tau_E, \end{cases} \tag{25}$$

where k_{sgn} is the sign of thrust bias direction, $\Delta\tau_E = \tau_e - \tau_0$ is the energy management time, and τ_{Tra} is the reversal compensation time, which is used to conduct approximate compensation for the inversion time brought by the control variation rate constraint. Equation (25) shows that thrust bias direction is the same with closed-loop command direction at initial time. The thrust bias direction is reversed when the time exceeds the set reversal time. The energy management can be ended when (26) is met:

$$S \le \varepsilon_S, \tag{26}$$

where ε_S is a small constant value. Equation (26) shows that energy management can be ended and converted to the closed-loop guidance when S is reduced to a certain value. Energy management related change curves are given as in Figures 6 and 7.

Figure 6 shows that different S can be converged to zero in expected time within the range of rocket velocity waste capability. The larger the exponential coefficient k is, the faster the S decay becomes. Figure 7 shows α_c change curves under the control constraint and the thrust bias inversion strategy.

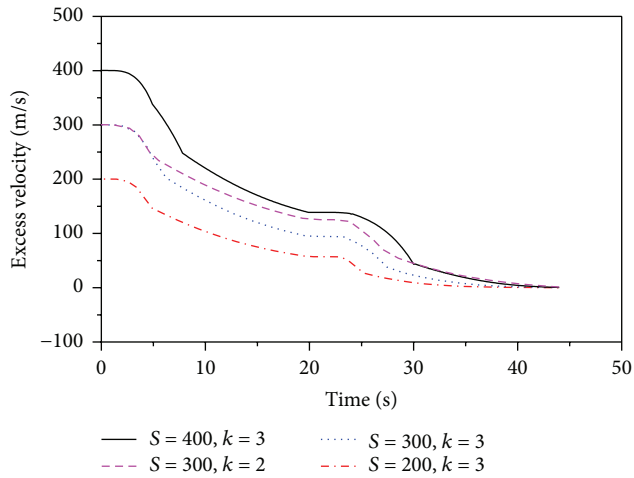

Figure 6: Excess velocity versus time.

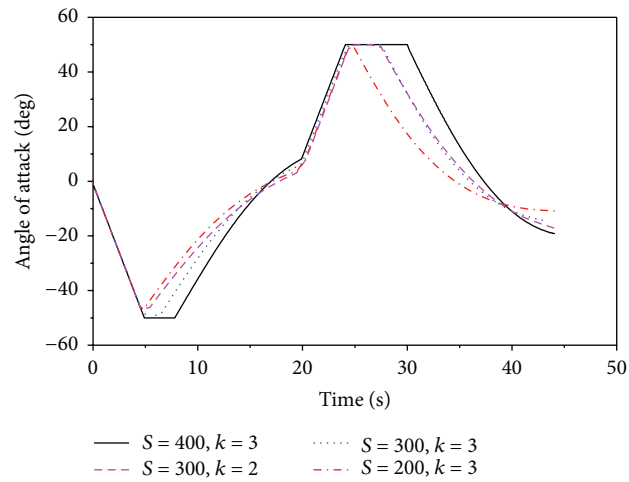

Figure 7: Angle of attack versus time.

The rocket is guaranteed to be at a reasonable position in space given that α_c contains the closed-loop guidance command.

The finished energy management can be converted to the closed-loop guidance. The different mission requirements indicate that corresponding spline guidance can be adopted. Cubic spline guidance can be used if no terminal angle of attack constraint exists. The quintic spline guidance can be utilized for its better continuity on control command than the quartic spline guidance when a terminal angle of attack constraint exists. The terminal velocity prediction is obtained by the cubic spline guidance. However, the influence of the control difference on terminal velocity is minimal under reasonable constraints. The multiconstrained closed-loop guidance flow chart is shown in Figure 8.

6. Simulation Results

This section conducts nominal and dispersion simulations to test the applicability and robustness of the multiconstrained

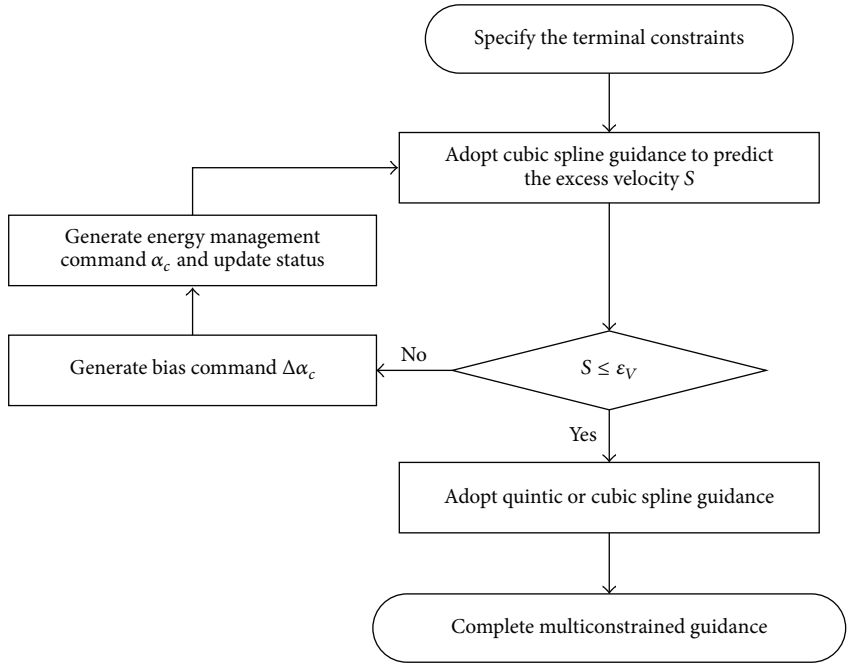

Figure 8: Flow chart of multiconstrained closed-loop guidance.

Table 2: Initial states.

h (km)	V (m/s)	γ (°)	α (°)
40	1671	18.3	0

Table 3: Terminal constraints.

	h_f^* (km)	α_f^* (°)	γ_f^* (°)	V_f^* (m/s)
Case 1	50	0	0	5000
Case 2	55	NAN	3	5100
Case 3	60	10	0	4900
Case 4	65	5	8	4800
Case 5	70	NAN	0	4950

closed-loop guidance method. The second-stage rocket is ignited when it reaches a suitable height. The initial states at the second-stage ignition time are shown in Table 2, and the five group terminal constraint conditions are presented in Table 3. The control constraints in the process of simulation are $|\alpha_c| \le 50^\circ$ and $|\dot{\alpha}_c| \le 10^\circ/\text{s}$. The energy management time is $\Delta\tau_E = 45$ s, and the exponential decay parameter is $k = 3$.

6.1. Nominal Cases. The cubic spline guidance in the closed-loop guidance phase is used for the cases (i.e., Cases 2 and 5) without a terminal angle of attack constraint. The others can adopt quintic spline guidance. Corresponding simulation results are indicated in Table 4 and Figures 9–12.

The simulation results show that this guidance algorithm can achieve the constraints of different terminal height, velocity, flight path angle, and angle of attack. Figure 9 shows the change of height under different terminal constraints. Figure 10 shows that the angle of attack change is relatively slight because its maximum angle and angular rate have been limited. The initial bias direction indicates that the initial closed-loop guidance command direction in Case

Table 4: Simulation results.

	h_f (m)	α_f (°)	γ_f (°)	V_f (m/s)
Case 1	50003	−0.14	−0.01	5004
Case 2	55001	4.89	2.99	5104
Case 3	60000	8.86	0.02	4894
Case 4	64994	4.72	7.99	4802
Case 5	69998	−11.87	0.00	4952

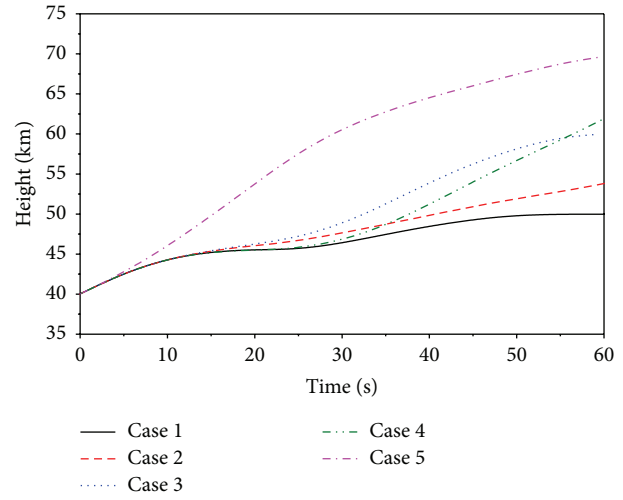

Figure 9: Height versus time.

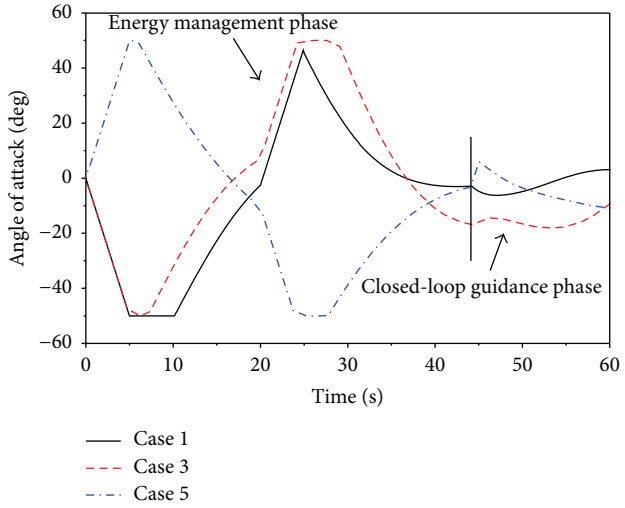

Figure 10: Angle of attack versus time.

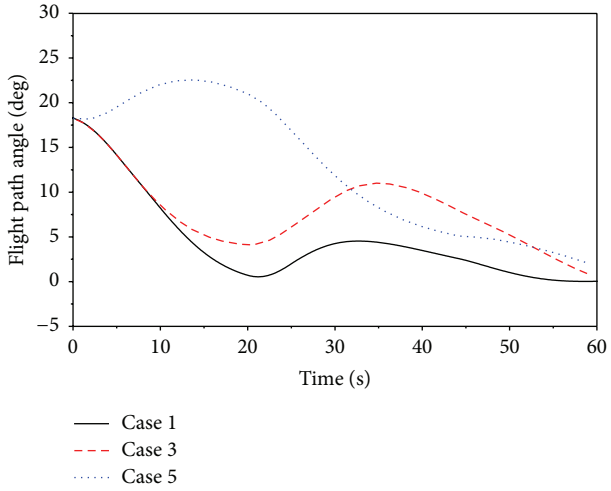

Figure 11: Angle of attack versus time.

5 is opposite to that in Cases 1 and 3. Cubic or quintic spline guidance in terminal closed-loop guidance phase is selected according to whether an angle of attack constraint requirement exists or not. Figure 11 proves that the change of the flight path angle is consistent with the change of guidance command. Figure 12 shows that the rocket can complete the dissipation of excess velocity at the desired time through energy management.

6.2. Dispersion Testing. To further test the guidance performance and robustness under a wide array of common random dispersions in ascent flight, Monte Carlo simulations are implemented 1,000 times for Case 3. The specific impulse, mass flow ratio, aerodynamic coefficients, and atmospheric density are all dispersed. The dispersions obey the Gaussian distribution and are shown in Table 5. The simulations statistical results are presented in Figure 13 and Table 6.

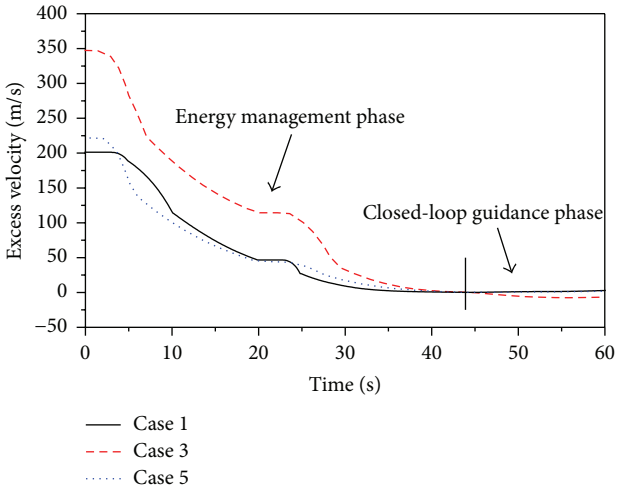

Figure 12: Excess velocity versus time.

Table 5: Dispersions used in Monte Carlo simulations.

Parameter	Mean	Value ($3-\sigma$)	Unit
Specific impulse	0	3	s
Mass flow ratio	0	5	%
Drag coefficient	0	20	%
Lift coefficient	0	20	%
Atmospheric density	0	20	%

Table 6: Monte Carlo simulations statistic results.

Terminal state deviation	Maximum/minimum	Mean	Standard deviation
$\Delta\gamma_f$ (°)	0.1127	0.0212	0.0268
Δh_f (m)	3.1650	0.4775	0.4546
ΔV_f (m/s)	−44.2075	−4.8080	12.7036
$\Delta\alpha_f$ (°)	−3.3150	−1.0896	0.7303
Δt_f (s)	−3.81	0.0698	1.0756

The simulation results show that the dispersion of terminal state deviation is well-distributed and within the reasonable range. Therefore, this algorithm possesses favorable robustness and can meet the guidance requirements under the influence of uncertainties.

7. Conclusions

This paper proposes a multiconstrained ascent guidance method for a solid rocket-powered launch vehicle, which takes a hypersonic glide vehicle as the load and shuts off by fuel exhaustion. The pseudospectral method is used to analyze ascent trajectory characteristics. Moreover, determining the "glide-insertion" launch trajectory with rocket "burn-coast-burn" ignition mode is suitable for such flight missions. Based on the characteristics of the second-stage rocket flight phase, a multiconstrained closed-loop guidance method based on spline curve and the corresponding bias energy management strategy are proposed. Finally, the nominal and

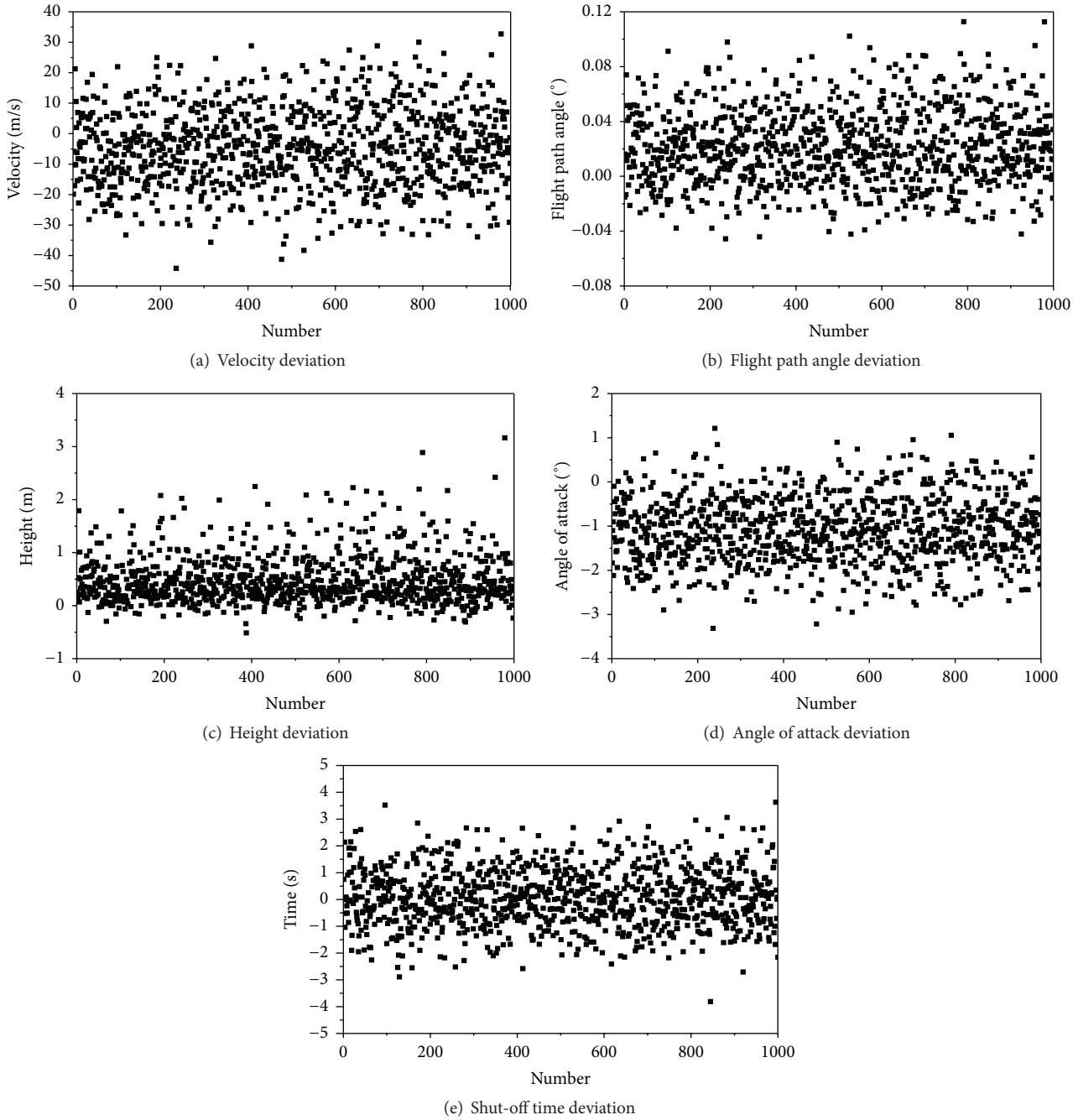

(a) Velocity deviation

(b) Flight path angle deviation

(c) Height deviation

(d) Angle of attack deviation

(e) Shut-off time deviation

Figure 13: Dispersion of terminal state deviation.

the dispersion simulations are used to verify the closed-loop guidance method. The simulation results prove the excellent applicability and robustness of this method, which can be used as a reference for the ascent trajectory design and guidance method of solid rocket-powered launch vehicles.

Competing Interests

The authors declare that there is no conflict of interests regarding the publication of this paper.

References

[1] S. H. Walker, J. Sherk, D. Shell, R. Schena, J. Bergmann, and J. Gladbach, "The DARPA/AF falcon program: the hypersonic technology vehicle #2 (HTV-2) flight demonstration phase," AIAA Paper 2008-2539, 2008.

[2] P. Lu, S. Forbes, and M. Baldwin, "Gliding guidance of high L/D hypersonic vehicles," AIAA Paper 2013-4648, 2013.

[3] J. T. Betts, "Survey of numerical methods for trajectory optimization," *Journal of Guidance, Control, and Dynamics*, vol. 21, no. 2, pp. 193–207, 1998.

[4] G. Brauer, D. Cornick, and R. Stevenson, *Capabilities and Applications of the Program to Optimize Simulated Trajectories (POST): Program Summary Document*, 1977.

[5] S. Paris and C. Hargraves, *OTIS 3.0 Manual*, vol. 24, Boeing Space and Defense Group, Seattle, Wash, USA, 1996.

[6] D. Benson, *A Gauss Pseudospectral Transcription for Optimal Control*, Massachusetts Institute of Technology, 2005.

[7] G. T. Huntington, D. Benson, and A. V. Rao, "A comparison of accuracy and computational efficiency of three pseudospectral methods," in *Proceedings of the AIAA Guidance, Navigation, and Control Conference*, vol. 6405 of *AIAA paper*, pp. 840–864, Hilton Head Island, SC, USA, August 2007.

[8] D. A. Benson, G. T. Huntington, T. P. Thorvaldsen, and A. V. Rao, "Direct trajectory optimization and costate estimation via an orthogonal collocation method," *Journal of Guidance, Control, and Dynamics*, vol. 29, no. 6, pp. 1435–1440, 2006.

[9] A. V. Rao, D. Benson, C. L. Darby et al., *User's Manual for GPOPS Version 5.0: A MATLAB Software for Solving Multiple-Phase Optimal Control Problems Using hp-Adaptive Pseudospectral Methods*, 2011.

[10] P. Lu, "Nonlinear trajectory tracking guidance with application to a launch vehicle," *Journal of Guidance, Control, and Dynamics*, vol. 19, no. 1, pp. 99–106, 1996.

[11] H. Seywald and E. M. Cliff, "Neighboring optimal control based feedback law for the advanced launch system," *Journal of Guidance, Control, and Dynamics*, vol. 17, no. 6, pp. 1154–1162, 1994.

[12] D. T. Martin, R. M. Obrien, A. F. Rice, and R. F. Sievers, "Saturn V guidance, navigation, and targeting," *Journal of Spacecraft and Rockets*, vol. 4, no. 7, pp. 891–898, 1967.

[13] R. L. McHenry, T. J. Brand, A. D. Long, B. F. Cockrell, and J. R. Thibodeau III, "Space Shuttle ascent guidance, navigation, and control," *Journal of the Astronautical Sciences*, vol. 27, no. 1, pp. 1–38, 1979.

[14] K. R. Brown and G. W. Johnson, "Real-time optimal guidance," *IEEE Transactions on Automatic Control*, vol. 12, no. 5, pp. 501–506, 1967.

[15] G. A. Dukeman, "Atmospheric ascent guidance for rocket-powered launch vehicles," in *Proceedings of the AIAA Guidance, Navigation, and Control Conference and Exhibit*, vol. 4559 of *AIAA Paper*, pp. 5–8, Monterey, Calif, USA, August 2002.

[16] G. Dukeman and A. J. Calise, "Enhancements to an atmospheric ascent guidance algorithm," AIAA Paper 2003-5638, 2003.

[17] G. A. Dukeman, *Closed-Loop Nominal and Abort Atmospheric Ascent Guidance for Rocket-Powered Launch Vehicles*, Georgia Institute of Technology, Atlanta, Ga, USA, 2005.

[18] P. Lu, H. Sun, and B. Tsai, "Closed-loop endoatmospheric ascent guidance," *Journal of Guidance, Control, and Dynamics*, vol. 26, no. 2, pp. 283–294, 2003.

[19] P. Lu and B. Pan, "Highly constrained optimal launch ascent guidance," *Journal of Guidance, Control, and Dynamics*, vol. 33, no. 2, pp. 404–414, 2010.

[20] R. H. Battin and R. M. Vaughan, "An elegant Lambert algorithm," *Journal of Guidance Control, and Dynamics*, vol. 1, no. 6, pp. 662–670, 1983.

[21] S. L. Nelson and P. Zarchan, "Alternative approach to the solution of Lambert's problem," *Journal of Guidance, Control, and Dynamics*, vol. 15, no. 4, pp. 1003–1009, 1992.

[22] G. Avanzini, "A simple lambert algorithm," *Journal of Guidance, Control, and Dynamics*, vol. 31, no. 6, pp. 1587–1594, 2008.

[23] J. T. Patha and R. K. McGehee, "Guidance, energy management, and control of a fixed-impulse solid-rocket vehicle during orbit transfer," in *Proceedings of the AIAA Guidance and Control Conference*, pp. 1–12, American Institute of Aeronautics and Astronautics, San Diego, Calif, USA, August 1976.

[24] P. Zarchan, *Tactical and Strategic Missile Guidance*, AIAA, Reston, Va, USA, 6th edition, 2012.

[25] P. H. Zipfel, "Orbital insertion control of a three-stage solid rocket booster modeled in six degrees-of-freedom," *Journal of Modeling, Simulation, Identification, and Control*, vol. 2, no. 1, pp. 31–44, 2014.

[26] H. Xu and W. Chen, "An energy management ascent guidance algorithm for solid rocket-powered launch vehicles," in *Proceedings of the 17th AIAA International Space Planes and Hypersonic Systems and Technologies Conference*, pp. 1–12, San Francisco, Calif, USA, April 2011.

[27] A. Tewari, *Advanced Control of Aircraft, Spacecraft and Rockets*, John Wiley & Sons, New York, NY, USA, 2011.

[28] M. J. Abrahamson, *Boost through Reentry Trajectory Planning for Maneuvering Reentry Vehicles*, Massachusetts Institute of Technology, 2007.

[29] T. H. Phillips, *A Common Aero Vehicle (CAV) Model, Description, and Employment Guide*, vol. 27, Schafer Corporation for AFRL and AFSPC, 2003.